

Submillimeter water and ammonia absorption by the peculiar $z \approx 0.89$ interstellar medium in the gravitational lens of the PKS 1830–211 system

K. M. Menten¹, R. Güsten¹, S. Leurini², S. Thorwirth¹, C. Henkel¹, B. Klein¹, C. L. Carilli³, and M. J. Reid⁴

¹ Max-Planck-Institut für Radioastronomie, Auf dem Hügel 69, 53121 Bonn, Germany
e-mail: [kmenten;rguesten;sthorwirth;chenkel;bklein]@mpi.fr-bonn.mpg.de

² ESO, Karl-Schwarzschild-Strasse 2, 85748 Garching bei München, Germany
e-mail: sleurini@eso.org

³ National Radio Astronomy Observatory, PO Box 0, Socorro, NM 87801-0387, USA
e-mail: ccarilli@nrao.edu

⁴ Harvard-Smithsonian Center for Astrophysics 60 Garden Street Cambridge, MA 02138, USA
e-mail: reid@cfa.harvard.edu

Received 24 April 2008 / Accepted 15 October 2008

ABSTRACT

Using the Atacama Pathfinder Experiment (APEX) telescope, we have detected the rotational ground-state transitions of ortho-ammonia and ortho-water toward the redshift ≈ 0.89 absorbing galaxy in the PKS 1830–211 gravitational lens system. We discuss our observations in the context of recent space-borne data obtained for these lines with the SWAS and Odin satellites toward Galactic sources. We find commonalities, but also significant differences between the interstellar media in a galaxy at intermediate redshift and in the Milky Way. Future high-quality observations of the ground-state ammonia transition in PKS 1830–211, together with inversion line data, will lead to strong constraints on the variation in the proton to electron mass ratio over the past 7.2 Gyr.

Key words. cosmology: observations – gravitational lensing – astrochemistry – ISM: abundances – ISM: molecules

1. Introduction

The gravitational lens system involving the bright compact radio and millimeter source PKS 1830–211 is remarkable for several reasons: a distant quasi-stellar object (QSO) at a redshift, z , of 2.507 (Lidman et al. 1999) is imaged into two strong, milliarc-second (mas) size sources separated by ≈ 970 mas, corresponding to 7.3 kpc at $z = 0.89^1$ (Jin et al. 2003). These components appear embedded in extended emission, part of which, at high resolution, presents an Einstein ring (Subrahmanyan et al. 1990; Jauncey et al. 1991).

Through an act of “cosmic conspiracy”, the line of sight to the background QSO passes through or near several galaxies (Meylan et al. 2005) and, placed at Galactic longitude $+12^\circ 2$ and latitude $-5^\circ 7$, the bulge of the Milky Way, causing local neutral hydrogen (HI) absorption (Subrahmanyan et al. 1992). Courbin et al. (2002) give a historical summary of this complex picture. Most importantly, the line of sight passes through a spiral galaxy at a redshift of ≈ 0.89 (Winn et al. 2002), in which continuum emission from the QSO is absorbed in lines of atomic hydrogen and hydroxyl (OH) (Chengalur et al. 1999; Koopmans & de Bruyn 2005) and transitions from a variety of molecules in the interstellar media of two different spiral arms (Wiklind & Combes 1996, 1998). The much deeper absorption has its centroid at $z = 0.88582$ (zero velocity in the heliocentric frame) and is toward the south-western (SW) image

(Frye et al. 1997; Muller et al. 2006), which is rendered undetectable at optical wavelengths by the dust mixed with the molecular material (Winn et al. 2002). The absorption appears to be caused by material in a spiral arm of the lensing galaxy at projected distance of $\approx 0'.4$ from the galaxy’s center (3 kpc), clearly defined in the I -image presented by these authors. We note that in the Milky Way the bulk of the molecular gas is distributed between Galactocentric radii of 4 and 7 kpc (Bronfman et al. 1988).

Wiklind & Combes (1998) detected a second, weaker absorption cloud with a velocity shifted by -147 km s⁻¹ ($z = 0.88489$) relative to the primary absorption and toward the NE image (Muller et al. 2006), whose location is displaced by $0'.59$ (4.4 kpc) from galaxy’s center.

For completeness, we mention that there is another HI absorber at $z = 0.19$ that absorbs the NE and, weaker, the SW image as well as part of PKS 1830–211’s extended emission (Lovell et al. 1996). The nature of this low opacity ($\tau_{\text{HI}} \sim 0.01$) system’s host is uncertain but possibly we are dealing with another intervening spiral galaxy of low surface brightness. No molecular absorption has been detected at this redshift (Wiklind & Combes 1998).

Wiklind and Combes detected absorption in CO and in a number of molecules with (much) higher dipole moments, namely HCN, HCO⁺, CS, and N₂H⁺ (Wiklind & Combes 1996, 1998). Menten et al. (1999) added C₂H, HC₃N, and C₃H₂ to this list. A number of rare isotopologues of C-, N-, O-, and S-bearing species were imaged by Muller et al. (2006), who found isotopic ratios differing from Milky Way values. Menten et al. (1999)

¹ Throughout this paper we are using a Λ cosmology with $H_0 = 73$ km s⁻¹ Mpc⁻¹, $\Omega_M = 0.28$, and $\Omega_\Lambda = 0.72$ (Spergel et al. 2007). 1 arcsec corresponds to 7.54 kpc.

compared PKS 1830–211’s molecular make-up with Galactic dark clouds and found many similarities. Recently, [Henkel et al. \(2008\)](#) observed a total of ten metastable inversion transitions of ammonia (NH_3) and found the observations to be consistent with 80–90% of the ammonia-bearing gas being warm (~ 80 K). Amazingly, to explain the intensities of the lines at high energy levels (up to 1000 K above the ground-state) they have to invoke a hot >600 K medium for which in the Milky Way the only known counterpart would be the Sgr B2 region near the Galactic center ([Huettemeister et al. 1995](#); [Wilson et al. 2006](#)).

Redshifted absorbers provide the possibility to detect spectral lines that are unobservable from the ground due to attenuation by the Earth’s atmosphere, namely low excitation water (H_2O) lines that cause the bulk of the terrestrial absorption. This was exploited by [Combes & Wiklind \(1997\)](#), who discovered absorption in the $1_{10}-1_{01}$ ground-state transition of ortho-water (o- H_2O) toward the “other” rich molecular intermediate-redshift ($z = 0.685$) system B0218+357. The terrestrial, pressure-broadened $1_{10}-1_{01}$ H_2O line near 557 GHz causes the broadest range of absorption in the Earth’s atmosphere below 1 THz, rendering the ± 50 GHz around it practically impossible to observe from the ground, even from the excellent 5100 m high site of the APEX telescope. Considerable effort was put in the investigation of this line in the Milky Way; it was a main motivation for two space missions, the Submillimeter Wave Astronomy Satellite (SWAS [Melnick et al. 2000](#)) and Odin ([Nordh et al. 2003](#); [Hjalmarson et al. 2003](#)). Among many other things, Odin also delivered the first astronomical detection of the 1_0-0_0 ground-state transition of ammonia, NH_3 , which near 572 GHz is also unobservable from the ground due to absorption from the 557 GHz H_2O line’s broad line wings.

Here we report the detection of the H_2O and the NH_3 ortho-ground-state rotational lines toward PKS 1830–211 with the APEX telescope². In Sect. 2 we describe the observations and data reduction. Our results are presented in Sect. 3 and their analysis in Sect. 4. Astrochemical implications of our study are discussed in Sect. 5.

2. Observations and data reduction

Our observations were made in 2007 July 2–5 under generally good weather conditions with APEX, the 12-m Atacama Pathfinder Experiment telescope ([Güsten et al. 2006](#)). Opacities at the observing frequencies (≈ 300 GHz) were between 0.02 and 0.12 throughout the observations and (single sideband) system temperatures between 240 and 390 K. We observed the ortho-ground state lines of water (H_2O) and ammonia (NH_3), namely the H_2O $J_{K_a K_c} = 1_{10}-1_{01}$ and the NH_3 $J_K = 1_0-0_0$ transitions. These were redshifted from their rest frequencies of 556936.00 ± 0.05 and 572498.1 ± 0.3 MHz to observing frequencies, ν , of 295328.3 and 303580.4 MHz, respectively. We assumed the redshift accurately determined from mm-/cm-wavelength absorption measurements, namely $z = 0.88582$. All spectra are presented with velocities in the heliocentric frame; add 12.1 km s^{-1} for LSR velocities.

Both lines were measured in the lower sideband (LSB) with the APEX 2a facility receiver ([Risacher et al. 2006](#)). Calibration was obtained using the chopper wheel technique, considering the different atmospheric opacities in the signal and image sidebands of the employed double sideband receivers. To ensure flat spectral baselines, the newly available wobbling secondary was

chopped with a frequency of 1.5 Hz and a throw of $100''$ about the cross elevation axis. The wobbler was operated in symmetric mode, which means that source and off position are interchanged between subsequent subscans, which cancels any asymmetries in the optical paths. Such observations deliver a reliable estimate of the continuum level. The radiation was analyzed with the MPIfR Fast Fourier Transform spectrometer, which provides 16 384 frequency channels over the 1 GHz intermediate frequency bandwidth ([Klein et al. 2006](#)). To increase the signal to noise ratio, the spectra were smoothed to effective velocity resolutions appropriate for the measured linewidths, i.e., 4.0 and 3.9 km s^{-1} for the H_2O and NH_3 lines, respectively. To check the telescope pointing, drift scans were made across the strong continuum sources Sgr B2 N, G10.47+0.03, Jupiter, and Mars. Pointing corrections were derived from these measurements. The pointing was found to be accurate to within $\approx 3''$, acceptable given the *FWHM* beam size, θ_B , which is $21''$ *FWHM* at 300 GHz.

We have converted our line intensities, measured with the chopper wheel technique, into a flux density, S , scale (i.e., in Jansky units), assuming the aperture efficiency observationally determined by [Güsten et al. \(2006\)](#) at 352 GHz and higher frequencies extrapolated to 300 GHz; 1 K of antenna temperature corrected for above the atmosphere corresponds to 37.7 Jy . We present our observed spectra in Fig. 1 with the continuum levels indicated (see Sect. 3.1). No baselines were subtracted from these spectra.

3. Results

3.1. Continuum intensities

In the double-sideband APEX 2a receiver, the two sidebands are 12 GHz apart and continuum emission from both sidebands is detected. The effective center frequencies for the determination of the continuum levels are 301.3 and 309.6 GHz, respectively, for the two sidebands. We determine continuum levels, S_C , of 1.73 Jy at the former and 1.65 Jy at the latter frequency, respectively. Given the absolute calibration uncertainties, which we estimate at 10%, the difference between the two measurements is not significant. Keeping in mind that PKS 1830–211 is highly variable, we note that our flux densities are higher than the 1.3 Jy measured with the Large APEX Bolometer Camera (LABOCA) shortly before our observations, i.e., in 2007 May ([Weiss and Schuller, personal communication](#)). The LABOCA’s effective (filter-averaged) frequency is 345 GHz, 49 GHz higher than the H_2O line frequency. If PKS 1830–211’s submillimeter flux did *not* vary between then and the time of our measurements, comparison of our and the LABOCA data shows that the trend of dropping flux with increasing frequency continues at least up to 345 GHz.

We estimate the uncertainties of our absolute flux density calibration and the systematic uncertainties in the optical depth determinations (see Sect. 3.3) to be $\approx 10\%$. This means that the uncertainties in the optical depth determinations are dominated by the limited signal-to-noise ratio of the line measurements.

3.2. The magnification ratio and covering factor

With our $\approx 20''$ *FWHM* beam we are detecting the sum of the continuum flux densities from the NE and the SW images. However, from interferometric imaging it is clear that observed absorption at zero velocity (relative to $z = 0.88582$) only arises toward the weaker SW image ([Frye et al. 1997](#); [Menten et al. 1999](#); [Muller et al. 2006](#)). Thus, we must correct the observed apparent optical depths to true optical depths taking this into

² APEX observations of the H_2O line toward PKS 1830–211 have been announced previously by [Wiklind & Combes \(2005\)](#).

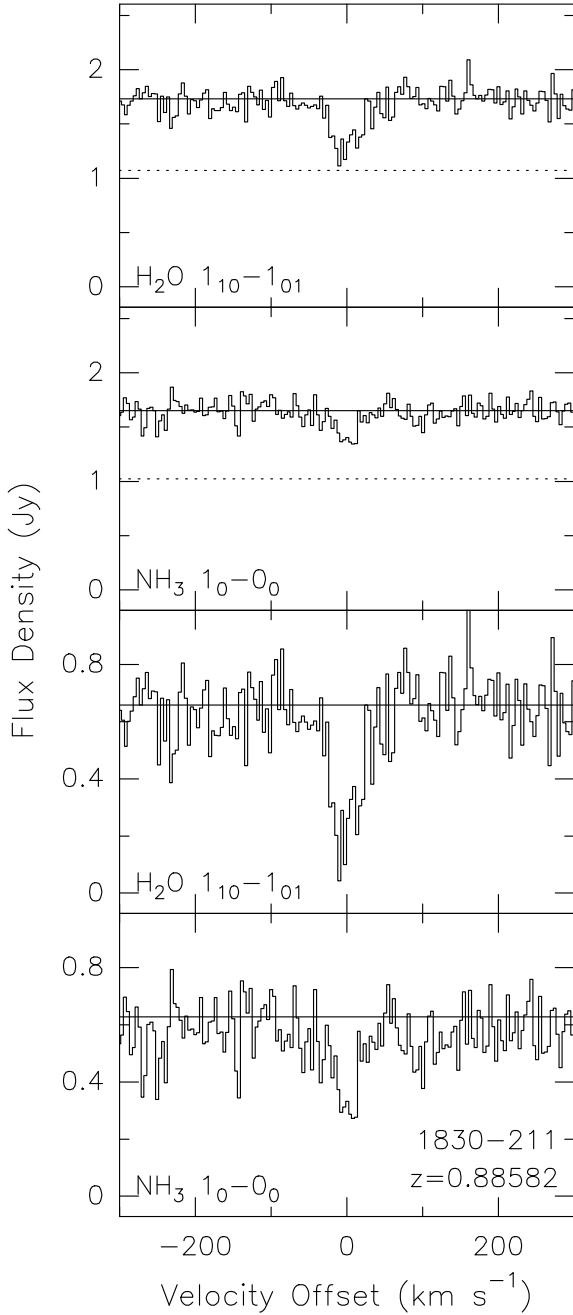


Fig. 1. Spectra of absorption in the $J_{K_a K_c} = 1_{10}-1_{01}$ transition of water vapor and the $J_K = 1_0-0_0$ transition of ammonia taken with the APEX telescope toward PKS 1830–211. The velocity scale is in the heliocentric frame and assumes a redshift of 0.88582. For the two upper spectra, the continuous horizontal line gives the continuum level discussed in Sect. 2 while the difference between the dotted and continuous lines gives the actually absorbed continuum level from the SW component (total covering factor 0.38; see Sect. 3.3). For clarity, in the lower panels the H₂O and NH₃ spectra are shown relative to the actually absorbed continuum level.

account. We here define the “magnification ratio”, \mathfrak{R} , for PKS 1830–211 as the ratio of the radio or (sub)millimeter flux densities of the stronger NE to the weaker SW image. Due to time delay between the two ray paths, this ratio is temporally variable, but if one accounts for that, $\mathfrak{R} \approx 1.5$ has been estimated in the radio regime (Lovell et al. 1998). Observations with the IRAM Plateau de Bure Interferometer (PdBI) taken between 1995 and 2003 in the 3 mm wavelength range show $\mathfrak{R} \approx 1.5-1.75$

(Muller et al. 2006), with a best value of 1.66. The flux density of the SW image is $\eta_{\text{cov}} S_C \equiv S_C / (1 + \mathfrak{R})$. Note that here the “covering factor” η_{cov} , which accounts for the fact that only the SW image is absorbed, ranges from 0.36 to 0.40, corresponding to the range in \mathfrak{R} given above. What fraction of that image’s few mas/few pc size area is absorbed is not considered and is assumed to be near unity as suggested by Very Long Baseline Array (VLBA) observations (Carilli et al. 1998).

3.3. Observed and corrected optical depths

A Gaussian fit to the H₂O line yields a peak line signal, S_L , of $-0.47(0.11)$ Jy, and an integrated line signal, $\int S_L dv$, of $-22.1(2.0)$ Jy km s⁻¹, an *FWHM* linewidth, Δv , of $44(5)$ km s⁻¹ and velocity offset, v , of $-1.8(2.0)$ km s⁻¹ relative to $z = 0.88582$. Using this line and the continuum flux density derived in Sect. 3.1 (10% uncertainty for the latter), we calculate an apparent optical depth,

$$\tau_{\text{app}} = -\ln(1 - |S_L|/S_C) \quad (1)$$

of $0.32_{-0.11}^{+0.15}$ and a velocity-integrated apparent optical depth, $\int \tau_{\text{app}} dv$ of 15.0 km s⁻¹.

For the NH₃ line we find $S_L = -0.29(6)$ Jy, $\int S_L dv = -10.4(1.6)$ Jy km s⁻¹, $\Delta v = 34(7)$ km s⁻¹, and $v = 0.5(2.5)$ km s⁻¹, yielding $\tau_{\text{app}} = 0.19_{-0.06}^{+0.08}$ and $\int \tau_{\text{app}} dv = 6.4$ km s⁻¹.

Replacing S_C with $\eta_{\text{cov}} S_C$ in the above equation and considering that $0.36 < \eta_{\text{cov}} < 0.40$, we obtain, for the H₂O line, a true optical depth of $1.3_{-0.6}^{+\infty}$ and 61 km s⁻¹ for its velocity-integrated value. This means that from our data we cannot give an upper bound for the line’s opacity.

For the NH₃ line we calculate $0.62_{-0.24}^{+0.46}$ and 22 km s⁻¹ for the true optical depth and its velocity-integrated value, respectively.

For a spectral line from an upper level u , with energy E_u , to a lower level l , with energy E_l , the column density in the upper level is

$$N_u = \frac{8\pi\nu^3}{c^3 A_{ul}} \left[e^{h\nu/kT_{\text{ex}}} - 1 \right]^{-1} \int \tau dv, \quad (2)$$

where T_{ex} is the excitation temperature, A_{ul} the Einstein *A* coefficient; h and k are the Planck and Boltzmann constants, respectively, and c is the speed of light. $\nu = (E_u - E_l)/h$ is the line’s rest frequency. In convenient units,

$$N_u(\text{cm}^{-2}) = 93.28 \frac{\nu^3(\text{GHz})}{A_{ul}(\text{s}^{-1})} \left[e^{0.048 \nu(\text{GHz})/T_{\text{ex}}(\text{K})} - 1 \right]^{-1} \times \int \tau dv (\text{km s}^{-1}). \quad (3)$$

The total column density is given by

$$N_{\text{rot}} = \frac{N_u}{g_u} e^{E_u/kT_{\text{rot}}} Q(T_{\text{rot}}), \quad (4)$$

where g_u is the line’s upper level degeneracy and Q is the partition function for the rotation temperature, T_{rot} . We assume Local Thermodynamic Equilibrium (LTE), which means $T_{\text{rot}} = T_{\text{ex}}$.

4. Analysis

4.1. Water vapor absorption

For the H₂O $J_{K_a K_c} = 1_{10}-1_{01}$ transition, $g_u = g_l = 9$ and $A_{ul} = 3.45 \times 10^{-3}$ s⁻¹, where u and l denote the 1_{10} and 1_{01}

energy levels, respectively. To consider the state of thermalization of this line, we examine the rates for collisional deexcitation from the 1_{01} level, which are accessible at the website of the Leiden Atomic and Molecular Database (LAMDA)³ (Schöier et al. 2005). The calculations of Grosjean et al. (2003) for collisions between ortho- H_2 and ortho- H_2O at low temperatures (5–20 K), extended to higher temperatures (140 K), using the results of Phillips et al. (1996), yield rate coefficients for transitions from the upper 1_{10} to the lower 1_{01} level, γ_{ul} , between 8.2×10^{-12} and $2.2 \times 10^{-11} \text{ cm}^3 \text{ s}^{-1}$ for kinetic temperatures between 5 and 80 K, where the latter number applies for the bulk of the gas from which absorption in the ammonia inversion transitions is also observed (Henkel et al. 2008). This implies a critical density, $n_{\text{crit}} = A_{ul}/\gamma_{ul}$, of several times 10^8 cm^{-3} , which is very much higher than any plausible value of the hydrogen density of the absorbing material. It is therefore straightforward to assume that the H_2O level populations are thermalized at the temperature of the cosmic microwave background, T_{CMB} . In other words, T_{ex} in Eq. (3) is equal to $T_{\text{CMB}} = (1+z) 2.728 \text{ K} = 5.145 \text{ K}$. Using these values and the lower limit to the integrated optical depth discussed in Sect. 3.3, i.e. $0.7 \times 39 = 27.3 \text{ km s}^{-1}$, with $T_{\text{ex}} = T_{\text{CMB}}$, Eq. (3) gives an upper level column density of $N_{1_{10}} = 7.1 \times 10^{11} \text{ cm}^{-2}$.

Noting that the ortho- H_2O partition function for this temperature, $Q_{\text{o-H}_2\text{O}}(5.145 \text{ K})$, is ≈ 9.05 , we can use Eq. (4) to find that the total ortho- H_2O column density, $N(\text{o-H}_2\text{O})$, is $9.9 \times 10^{13} \text{ cm}^{-2}$, 182.14 times higher than $N_{1_{10}}$ and, from detailed balance, that almost all ortho- H_2O molecules (99.45%) are in the 1_{01} ground-state level! To verify this, we used the non-LTE radiative transfer program RADEX⁴ created and made available to the community by van der Tak et al. (2007) to perform statistical equilibrium calculations. For a set of input excitation conditions, namely background temperature (5.145 K), kinetic temperature, and H_2 density, RADEX calculates level populations with column density and line width as radiative transfer input parameters and returns the excitation temperatures and optical depths of user-selected spectral lines.

Running RADEX, we find that for densities up to 10^6 cm^{-3} the excitation temperature does not become significantly higher than T_{CMB} . For the line width derived in Sect. 3 RADEX returns the optical depth value discussed above ($\tau = 0.7$) for an ortho- H_2O column density of $9.3 \times 10^{13} \text{ cm}^{-2}$, close to above estimate. This result is independent of all plausible values of the kinetic temperature and densities up to 10^6 cm^{-3} .

We emphasize that the above estimate is calculated for the lower limit of the true integrated optical depth derived in Sect. 3.3 and a strict lower limit. The upper uncertainty bound of the optical depth is not determinable from our noisy data.

4.2. Ammonia absorption

For the NH_3 $J_K = 1_0-0_0$ transition, $g_u = 12$ and for the $(J, K) = (1, 1)$ transition $g_u = 6$. These values include factors for nuclear spin degeneracies. The very different Einstein A coefficients for these lines are $A_{1_0-0_0} = 1.61 \times 10^{-3} \text{ s}^{-1}$ and $A_{1,1} = 1.71 \times 10^{-7} \text{ s}^{-1}$, respectively.

Deexcitation rates for collisions of H_2 with ortho- NH_3 have been calculated by Danby et al. (1988) and are also accessible at the LAMDA website. We find that the rate for collisional deexcitation, γ_{01} , from the 1_0 to the 0_0 level for temperatures between 15 and 300 K varies little and is between 4.3×10^{-11}

and $6.2 \times 10^{-11} \text{ cm}^3 \text{ s}^{-1}$. The critical density of the $J_K = 1_0-0_0$ transition, $n_{\text{crit}}(1_0-0_0) = A_{ul}/\gamma_{ul}$, is, thus, $\sim 3 \times 10^7 \text{ cm}^{-3}$, which is, as in the case of the H_2O line discussed above, many orders of magnitude higher than the densities (of order a few times 10^3 cm^{-3}) of the absorbing interstellar medium (ISM) in PKS 1830–211. It is therefore also clear that the population of the NH_3 1_0 relative to the 0_0 level is controlled by the cosmic microwave background temperature. Using Eq. (3), we calculate $N_{1_0} = 1.4 \times 10^{12} \text{ cm}^{-2}$ for the column density of the 1_0 level. We can calculate the ortho- NH_3 partition function by direct summation with parameters from LAMDA and get, assuming $T_{\text{rot}} = 5.145 \text{ K}$, $Q_{\text{o-NH}_3}(5.145 \text{ K}) \approx 4.06$. Using Eq. (4) we find that the total ortho- NH_3 column density, $N(\text{o-NH}_3)$, is $9.1 \times 10^{13} \text{ cm}^{-2}$, 70 times higher than N_{1_0} .

Again using RADEX, we find that to reproduce our observed opacity (0.62 at a line width of 34 km s^{-1}) requires an ortho-ammonia column density, $N(\text{o-NH}_3)$, of $1.3 \times 10^{14} \text{ cm}^{-2}$. For $T_{\text{rot}} = 5.145 \text{ K}$, a quarter of all ortho- NH_3 molecules are in the 0_0 ground-state level while, in contrast to o- H_2O , the majority of molecules are in other energy levels. We used a kinetic temperature of 80 K (see Sect. 1 and Henkel et al. 2008) but note that lower temperatures would only imply a 20% lower column density at the most.

5. Discussion – Abundances and astrochemical implications

To calculate molecular abundances relative to molecular hydrogen, we assume an H_2 column density of $3 \times 10^{22} \text{ cm}^{-2}$ for the absorbing material toward PKS 1830–211-SW. This value was estimated by Wiklind & Combes (1996) assuming a CO to H_2 ratio of 10^{-4} . It is somewhat larger than the $(1.8 \pm 0.3) \times 10^{22} \text{ cm}^{-2}$ derived from X-ray observations with the ROSAT satellite (Mathur & Nair 1997).

With the lower limit to $N(\text{o-H}_2\text{O})$ determined above, $1.2 \times 10^{14} \text{ cm}^{-2}$, we find that the ortho- H_2O to H_2 abundance ratio, $X(\text{o-H}_2\text{O})$, is greater than $\approx 5 \times 10^{-9}$. To put this value into context, SWAS observed the same H_2O line in a wide variety of Galactic sources (for an overview see Melnick et al. 2000). Snell et al. (2000a) were able to determine H_2O abundances, with values similar to our PKS 1830–211 number, toward dense quiescent regions of molecular clouds (between 6×10^{-10} and 1×10^{-8}), with values near the higher number found in the core regions of Giant Molecular Clouds (GMCs, see also Bergin et al. 2000).

Several observational effects have to be considered concerning the SWAS results: the regions toward which SWAS detected the H_2O line at low abundance are core regions of molecular clouds, some of them GMCs, i.e., regions of enhanced density and thus, enhanced column density, producing high enough optical depths to make the line detectable. They are quiescent in the sense they do not harbor outflows. Whereas toward the spatially confined regions harboring outflows, as indicated by broad line wings and other tracers, SWAS finds several orders of magnitude higher H_2O abundances (Bergin et al. 2000, 2003). Similarly, higher H_2O abundances are found near the warmer interfaces to HII regions (Snell et al. 2000b). SWAS gives little information, just rough upper limits, on water in the lower density extended gas of giant molecular clouds, simply because the expected line intensities are prohibitively low. Similarly, only coarse upper limits (around 10^{-7} – 10^{-6} relative to H_2) can be derived toward cold dark clouds such as TMC-1, L134N, or B335, which also have lower average densities (10^4 cm^{-4}) than warm GMC cores. Moreover, their low temperatures (10 K) are not

³ <http://www.strw.leidenuniv.nl/~moldata/>

⁴ <http://www.strw.leidenuniv.nl/~moldata/radex.html>

conductive for producing emission in the $1_{10}-1_{01}$ line, whose upper energy level is 34 K above ground.

The size of the $\sim 4'$ FWHM beam of SWAS at the H_2O line rest frequency (557 GHz) for a region at distance D (measured in kpc) corresponds to an area of size $\approx 1 \text{ pc} \times D(\text{kpc})$. This means that for sources at a few kpc distance, similar size scales are sampled as for PKS 1830–211 with the VLBA beam of Carilli et al. (1998), which has a FWHM of 1 mas (7.5 pc at $z = 0.89$). Indeed, the SWAS H_2O spectrum of the W 33 region, which is at a (near-kinematic) distance of 4 kpc, has a width of $\sim 25 \text{ km s}^{-1}$ full width at zero power (FWZP)⁵. This is very wide for a quiescent cloud core which, as the low H_2O abundance suggests, does not contain outflows. The width could be determined by a combination of the presence of velocity gradients in the region unresolved by the beam and the existence of emission from several spiral arms caused by the line of sight crossing the plane of the Galaxy. Alternately, an outflow could be present, which actually is suggested by emission from the outflow tracer SiO from which lines of width comparable to the H_2O line's are observed toward W33 (Miettinen et al. 2006). In that case, the apparent low H_2O abundance could result from the superposition of a compact (i.e. beam diluted) higher-abundance outflow component and a more extended component of much lower abundance.

Even in comparison to the relatively broad H_2O emission toward W33, the 55–60 km s^{-1} FWZP width of the PKS 1830–211-SW absorption appears *extraordinarily* broad, especially since we are viewing the lensing galaxy close to face-on and the 2 milliarcsec size absorption “pencil beam” afforded by the size of the background source corresponds to a scale of 15 pc, smaller than a single GMC. Interferometric observations of the local face-on spiral M 51 with a resolution corresponding to a much larger $\sim 150 \text{ pc}$ reveal linewidths only between 10 and 20 km s^{-1} in the galaxy's spiral arms (Aalto et al. 1999).

The probability of a random line of sight passing through a cloud core certainly is lower than passing through a lower density, more “normal”, region of a GMC. The H_2O abundance in the bulk volume of molecular clouds is essentially unknown and, for the above reasons, SWAS or ODIN cannot deliver very meaningful limits. As the multi-molecule studies of galactic absorption against extragalactic radio sources conducted by Liszt and Lucas have persuasively demonstrated, all the other molecules found toward PKS 1830–211 can be detected in general molecular ISM gas (Lucas & Liszt 2000; Liszt & Lucas 2001; Liszt et al. 2004; Liszt & Lucas 2004; Liszt et al. 2006). However, as explained in the following, the gas absorbing PKS 1830–211 appears to have a much higher temperature.

Using the NRAO Green Bank Telescope, Henkel et al. (2008) detected absorption in the NH_3 (J, K) inversion lines toward PKS 1830–211 for $J = K = 1$ up to 10, which arise from levels with energies between 23 and 1036 K above ground. Figure 2 compares our spectrum of the $J_K = 1_1-0_0$ line with their $J, K = (1, 1)$ spectrum. There appears to be excess absorption in the former at velocities $>0 \text{ km s}^{-1}$, although the signal-to-noise ratio is rather limited. If real, this would be difficult to explain since, given that the absorbed region is larger at the redshifted (1, 1) frequency (12.56 GHz) than at the 1_1-0_0 frequency, one would expect the opposite. Higher signal to noise data obtainable with the Submillimeter Array seem highly desirable!

Henkel et al. (2008) find that to explain the observed inversion line optical depths, 80–90% of the NH_3 must be in warm

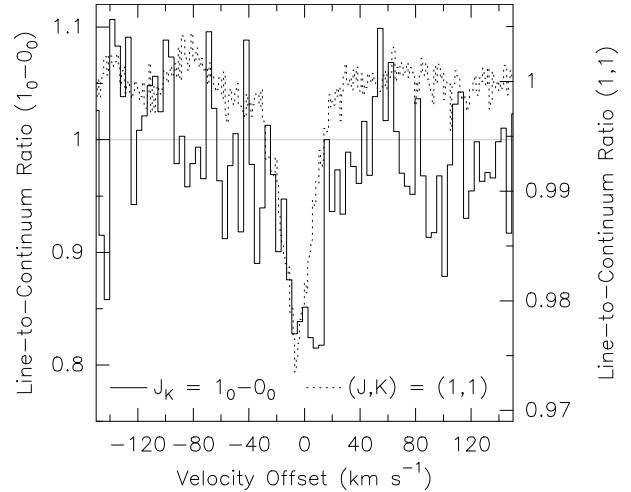


Fig. 2. Ammonia absorption spectra of the $J_K = 1_0-0_0$ rotational transition (full line) and the $(J, K) = (1, 1)$ inversion transition (dashed line) toward PKS 1830–211. The velocity scale is in the heliocentric frame and assumes a redshift of 0.88582. The y -axes give the line-to-continuum ratio for the 1_0-0_0 line (left), for which the continuum level is 1.65 Jy, and the (1, 1) line (right) for which the continuum level is 8.2 Jy.

(80 K) gas with a total ortho- plus para- NH_3 column density of $5 \times 10^{14} \text{ cm}^{-2}$, if the excitation temperature (assumed to be the same for all lines) equals T_{CMB} . When modeling the clouds in their SWAS sample, Snell et al. (2000b) assumed temperatures between 25 and 40 K for the GMC cores, as determined from observations of other tracers, which is significantly lower than the 80 K quoted above. Moreover, the kinetic temperatures of 25–30 K derived by Liszt et al. (2006) from the NH_3 (1, 1) and (2, 2) lines are substantially lower. This poses an interesting question: is the $z = 0.89$ absorbing cloud much hotter than Galactic clouds or could a dilute warm molecular component in the Milky Way (and other galaxies) so far have escaped observational attention?

The ortho- NH_3 column density determined by us is a factor of 2 lower than the value derived from inversion lines (Henkel et al. 2008). Interestingly, a *much larger* discrepancy seems to exist between the NH_3 column density derived from the Odin 1_1-0_0 spectrum (Liseau et al. 2003) and the much higher value implied by the (1, 1) and (2, 2) inversion lines mapped by Zeng et al. (1984) toward the dark cloud ρ Oph A.

6. Outlook – constraints on variation of fundamental constants

Comparing the redshifts of various spectral lines measured toward the same high- z object can in principle yield constraints on possible temporal variations of fundamental constants over significant parts of the age of the Universe (see, e.g. Curran et al. 2004). A precondition is that the lines in question have different dependencies on the constants, e.g., the fine structure constant, α , and/or the ratio of the mass of the proton to that of the electron, $\mu = m_p/m_e$. Traditionally exploited with optical/UV quasar absorption lines, the method has recently been applied to radio and millimeter absorption lines toward, amongst others, the gravitational lens systems PMN J0134–0931 (Kanekar et al. 2005) and B0218+357 (Murphy et al. 2008).

The ammonia molecule is especially interesting with respect to this, as its inversion transitions are strongly dependent on μ : Flambaum & Kozlov (2007) find that the fractional change in

⁵ Intriguingly, the W33 spectrum shows absorption against the source's strong submillimeter continuum emission in its central velocity range.

frequency of these transitions $\delta v_{\text{inv}}/v_{\text{inv}} = \delta z/(1+z)$ is given by $-4.46\delta\mu/\mu$ or, in other words, $\Delta v_{\text{inv}} \propto \Delta\mu^{-4.46}$. For fractional variations of rotational line frequencies, v_{rot} , in contrast, the proportionality factor is unity, i.e., $\delta v_{\text{rot}}/v_{\text{rot}} = -\delta\mu/\mu$. Comparing NH_3 inversion line redshifts with redshifts of rotational lines should thus provide sensitive limits on the variation of μ .

Murphy et al. (2008) compare the measured redshifts of the NH_3 (J, K) = (1, 1), (2, 2) and (3, 3) lines observed toward B0218+357 by Henkel et al. (2005) with rotational lines from HCO^+ and HCN and obtain $\delta\mu/\mu = (0.74 \pm 0.47) \times 10^{-6}$ over a look-back time of 6.2 Gyr, corresponding to the absorber's redshift of 0.68466. One fundamental limitation of this measurement is the uncertainty over the two species' possibly different distributions leading to different covering factors. Different covering factors might also result from source size variations between 14 GHz (NH_3) and 105 GHz (HCO^+ and HCN). In addition, lines from different species might also cover different velocity ranges.

The ortho-ground-state rotational transition of NH_3 we have detected toward PKS 1830–211 can in principle deliver a more accurate and meaningful comparison between the redshifts of a rotational line redshift and of the inversion lines, which have been determined by Henkel et al. (2008, see Sect. 1). The velocity accuracy of our APEX measurement (2.5 km s^{-1}) translates into a redshift uncertainty, δz , of 1.6×10^{-5} and a value of $\delta\mu/\mu \approx 0.224 \delta z/(1+z)$ of 1.9×10^{-6} , which is three times larger than the value derived by Murphy et al. (2008) for B0218+357.

Our NH_3 1_0-0_0 spectrum is of very limited quality and even looks quite different from the (1, 1) spectrum (see Fig. 2), although that can be attributed to the former line's poor signal-to-noise ratio. A few hour long observation with the Submillimeter Array (Ho et al. 2004) will result in a much improved spectrum, which, together with the (1, 1) spectrum could lead to a significant advancement in investigating the variation of μ over the past 7.2 Gyr.

Acknowledgements. We would like to thank Gary Melnick for useful comments on this paper.

References

- Aalto, S., Hüttemeister, S., Scoville, N. Z., & Thaddeus, P. 1999, *ApJ*, 522, 165
 Bergin, E. A., Melnick, G. J., Stauffer, J. R., et al. 2000, *ApJ*, 539, L129
 Bergin, E. A., Kaufman, M. J., Melnick, G. J., Snell, R. L., & Howe, J. E. 2003, *ApJ*, 582, 830
 Bronfman, L., Cohen, R. S., Alvarez, H., May, J., & Thaddeus, P. 1988, *ApJ*, 324, 248
 Carilli, C. L., Menten, K. M., Reid, M. J., Rupen, M., & Claussen, M. 1998, in *Radio Emission from Galactic and Extragalactic Compact Sources*, ed. J. A. Zensus, G. B. Taylor, & J. M. Wrobel, IAU Colloq., 164, ASP Conf. Ser., 144, 317
 Chengalur, J. N., de Bruyn, A. G., & Narasimha, D. 1999, *A&A*, 343, L79
 Combes, F., & Wiklind, T. 1997, *ApJ*, 486, L79
 Courbin, F., Meylan, G., Kneib, J.-P., & Lidman, C. 2002, *ApJ*, 575, 95
 Curran, S. J., Kanekar, N., & Darling, J. K. 2004, *New Astron. Rev.*, 48, 1095
 Danby, G., Flower, D. R., Valiron, P., Schilke, P., & Walmsley, C. M. 1988, *MNRAS*, 235, 229
 Flambaum, V. V., & Kozlov, M. G. 2007, *Phys. Rev. Lett.*, 98, 240801
 Frye, B., Welch, W. J., & Broadhurst, T. 1997, *ApJ*, 478, L25
 Grosjean, A., Dubernet, M.-L., & Ceccarelli, C. 2003, *A&A*, 408, 1197
 Güsten, R., Nyman, L. Å., Schilke, P., et al. 2006, *A&A*, 454, L13
 Henkel, C., Jethava, N., Kraus, A., et al. 2005, *A&A*, 440, 893
 Henkel, C., Braatz, J. A., Menten, K. M., & Ott, J. 2008, *A&A*, 485, 451
 Hjalmarsen, Å., Frisk, U., Olberg, M., et al. 2003, *A&A*, 402, L39
 Ho, P. T. P., Moran, J. M., & Lo, K. Y. 2004, *ApJ*, 616, L1
 Huettemeister, S., Wilson, T. L., Mauersberger, R., et al. 1995, *A&A*, 294, 667
 Jauncey, D. L., Reynolds, J. E., Tzioumis, A. K., et al. 1991, *Nature*, 352, 132
 Jin, C., Garrett, M. A., Nair, S., et al. 2003, *MNRAS*, 340, 1309
 Kanekar, N., Carilli, C. L., Langston, G. I., et al. 2005, *Phys. Rev. Lett.*, 95, 261301
 Klein, B., Philipp, S. D., Krämer, I., et al. 2006, *A&A*, 454, L29
 Koopmans, L. V. E., & de Bruyn, A. G. 2005, *MNRAS*, 360, L6
 Lidman, C., Courbin, F., Meylan, G., et al. 1999, *ApJ*, 514, L57
 Liseau, R., Larsson, B., Brandeker, A., et al. 2003, *A&A*, 402, L73
 Liszt, H., & Lucas, R. 2001, *A&A*, 370, 576
 Liszt, H., & Lucas, R. 2004, *A&A*, 428, 445
 Liszt, H., Lucas, R., & Black, J. H. 2004, *A&A*, 428, 117
 Liszt, H. S., Lucas, R., & Pety, J. 2006, *A&A*, 448, 253
 Lovell, J. E. J., Reynolds, J. E., Jauncey, D. L., et al. 1996, *ApJ*, 472, L5
 Lovell, J. E. J., Jauncey, D. L., Reynolds, J. E., et al. 1998, *ApJ*, 508, L51
 Lucas, R., & Liszt, H. S. 2000, *A&A*, 358, 1069
 Mathur, S., & Nair, S. 1997, *ApJ*, 484, 140
 Melnick, G. J., Stauffer, J. R., Ashby, M. L. N., et al. 2000, *ApJ*, 539, L77
 Menten, K. M., Carilli, C. L., & Reid, M. J. 1999, in *Highly Redshifted Radio Lines*, ed. C. L. Carilli, S. J. E. Radford, K. M. Menten, & G. I. Langston, ASP Conf. Ser., 156, 218
 Meylan, G., Courbin, F., Lidman, C., Kneib, J.-P., & Tacconi-Garman, L. E. 2005, *A&A*, 438, L37
 Miettinen, O., Harju, J., Haikala, L. K., & Pomré, C. 2006, *A&A*, 460, 721
 Muller, S., Guélin, M., Dumke, M., Lucas, R., & Combes, F. 2006, *A&A*, 458, 417
 Murphy, M. T., Flambaum, V. V., Muller, S., & Henkel, C. 2008, *Science*, 320, 1611
 Nordh, H. L., von Schéele, F., Frisk, U., et al. 2003, *A&A*, 402, L21
 Phillips, T. R., Maluendes, S., & Green, S. 1996, *ApJS*, 107, 467
 Risacher, C., Vassilev, V., Monje, R., et al. 2006, *A&A*, 454, L17
 Schöier, F. L., van der Tak, F. F. S., van Dishoeck, E. F., & Black, J. H. 2005, *A&A*, 432, 369
 Snell, R. L., Howe, J. E., Ashby, M. L. N., et al. 2000a, *ApJ*, 539, L97
 Snell, R. L., Howe, J. E., Ashby, M. L. N., et al. 2000b, *ApJ*, 539, L101
 Spergel, D. N., Bean, R., Doré, O., et al. 2007, *ApJS*, 170, 377
 Subrahmanyam, R., Narasimha, D., Pramesh-Rao, A., & Swarup, G. 1990, *MNRAS*, 246, 263
 Subrahmanyam, R., Kesteven, M. J., & Te Lintel Hekkert, P. 1992, *MNRAS*, 259, 63
 van der Tak, F. F. S., Black, J. H., Schöier, F. L., Jansen, D. J., & van Dishoeck, E. F. 2007, *A&A*, 468, 627
 Wiklind, T., & Combes, F. 1996, *Nature*, 379, 139
 Wiklind, T., & Combes, F. 1998, *ApJ*, 500, 129
 Wiklind, T., & Combes, F. 2005, in *BAAS*, 37, 1424
 Wilson, T. L., Henkel, C., & Hüttemeister, S. 2006, *A&A*, 460, 533
 Winn, J. N., Kochanek, C. S., McLeod, B. A., et al. 2002, *ApJ*, 575, 103
 Zeng, Q., Batrla, W., & Wilson, T. L. 1984, *A&A*, 141, 127